http://dx.doi.org/10.5012/bkcs.2011.32.9.3333

Mechanochemical Synthesis of $ZnMn_2O_4$ and its Electrochemical Properties as an Anode Material for Lithium-ion Batteries

Yoon-Soo Park, Hoon Oh, and Sung-Man Lee*

*Department of Advanced Materials Science and Engineering, Kangwon National University, Chuncheon, Kangwon-Do 200-701, Korea. *E-mail: smlee@kangwon.ac.kr*
Received June 30, 2011, Accepted July 21, 2011

$ZnMn_2O_4$ has been prepared by a mechanochemical process using a mixture of Mn_2O_3 and ZnO as starting materials, and investigated as a possible anode material for lithium-ion batteries. The phase evolution and morphologies of the ball-milled and annealed powders are characterized by X-ray diffraction (XRD) and scanning electron microscopy (SEM) with energy dispersive microanalysis (EDX), respectively. The solid-state reaction for the formation of $ZnMn_2O_4$, under the given experimental conditions, is achieved in a short time (30 min), and the prepared samples exhibit excellent electrochemical performances including an enhanced initial coulombic efficiency, high reversible capacity, and stable capacity retention with cycling.

Key Words : Zinc-manganate, Mechanochemical process, Anode material, Lithium-ion battery

Introduction

Graphite is currently used as the anode material in lithium-ion batteries. However, as the theoretical capacity of graphite is limited to 372 mAh g^{-1}, seeking alternative anode materials for graphite is a primary concern for the development of lithium-ion batteries with high specific energy densities. Various anode materials, typically Si (or Sn)-containing alloys and composites, have been studied.

Recently, nanostructured transition metal oxides have attracted much attention as potential high capacity anode materials.[1-8] In particular, $ZnMn_2O_4$ is interesting because it is composed of cheap and non-toxic elements. $ZnMn_2O_4$ has been prepared by liquid-phase processes such as polymer-pyrosis[9] and solvothermal methods.[10]

Mechanochemical methods have been widely applied in the production of ceramics and alloys owing to their simplicity and relatively low costs.[11] In mechanochemical processing, mechanical energy is transferred to the particles and creates deformation and fractures on the surfaces, which cause thermodynamic and kinetic reactions between the particles, and chemical bonds are broken and new bonds are formed. A product obtained *via* the mechanochemical process usually contains defects and some disorder in the crystalline structure. However, considering that the $ZnMn_2O_4$ becomes amorphous during the first lithiation reaction and the amorphous nature is preserved during the charge-discharge cycles,[10] a pure crystalline product is not needed; therefore, it is worthwhile to explore $ZnMn_2O_4$ with its defective crystalline structure as an anode material for lithium-ion batteries.

In this work, $ZnMn_2O_4$ is prepared by mechanochemical synthesis and its electrochemical performance as the anode material in lithium-ion batteries is investigated. A well-crystallized $ZnMn_2O_4$ is obtained by annealing the mechanochemical sample and its electrochemical properties are measured and compared to the non-annealed sample.

Experimental

Mn_2O_3 (Aldrich, 99.9%) and ZnO (Cerac, 99.9%) were used as starting materials. The mechanochemical synthesis was performed on a planetary type high-speed ball-milling apparatus with a water cooling system at a rotation speed of 800 rpm for 10, 20, 30, and 40 min. The mixture of raw materials (in a 1:1 molar ratio) was loaded into a hardened steel vial, under atmospheric conditions with 7.9 mm diameter stainless steel balls. The ball to powder mass ratio was 15:1. Annealing of the as-milled powder was carried out in air at 600 °C for 2 h. The phase evolution of the ball-milled and annealed powders was characterized by X-ray diffraction (XRD) with Cu Kα radiation. The morphologies of the samples were observed by scanning electron microscopy (SEM) with energy dispersive microanalysis (EDX).

The size distribution of the particles was measured using a laser diffraction size analyzer. The electrochemical measurements were conducted in CR2016 half cells using a lithium metal foil as a counter electrode. Half-cells were assembled in an argon-filled glove-box. The electrodes were prepared by pasting a slurry containing 70 wt % active materials, 20 wt % carbon black, and 10 wt % polyvinyldene fluoride (PVDF) as a binder, dissolved in *N*-methyl-2-pyrrolidone (NMP) onto a copper foil. The electrodes were dried at 120 °C under vacuum overnight and then pressed. The electrolyte was 1 M $LiPF_6$ in a mixture of ethylene carbonate (EC) and diethyl carbonate (DEC) (1:1, v/v, provided by Panax Etec Co., Ltd., Korea). The cells were charged (lithiation) and discharged (delithiation) in the galvanostatic mode at a constant current of 100 $mAmg^{-1}$ in the voltage range 0.01-3.0 V.

Results and Discussion

Figure 1 shows the XRD patterns of the equimolar mixture of ZnO and Mn_2O_3 powders after different milling times. After 10 min milling, the diffraction peak intensities of the starting materials decrease and become significantly broader. The peaks of the $ZnMn_2O_4$ phase are visible after 20 min milling. After 30 min milling, the characteristic peaks corresponding to a tetragonal $ZnMn_2O_4$ structure appear on the XRD spectra, and they are extremely broad owing to fine particle sizes, lattice strains, and crystal defects. Higher milling times (40 min) lead to a slightly better crystallization of the $ZnMn_2O_4$ phase. It is noticeable that the $ZnMn_2O_4$ powders are synthesized successfully in the short milling time of 30 min. After heat treatment of the ball-milled powders at 600 °C in air for 2 h, a well-crystallized $ZnMn_2O_4$ phase is obtained, as shown by the sharp XRD peaks of the annealed product (Fig. 2). EDX analysis confirmed that the atomic ratio Zn/Mn is constant, within experimental error, from one particle to the other and corresponds well to the starting composition. In addition to the elements of the starting materials, EDX also revealed that the Fe contamination, arising from vial and balls debris, was about 0.4 and 1.2 at. % after 30 and 40 min of milling, respectively. SEM micrographs of the starting materials, the ball-milled

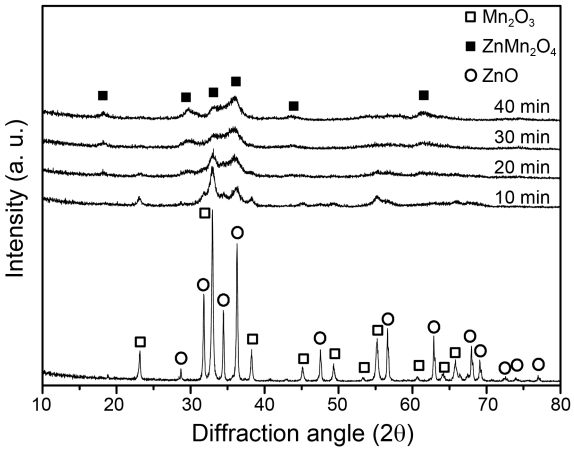

Figure 1. XRD patterns of the equimolar ZnO and Mn_2O_3 powder mixture after different milling times.

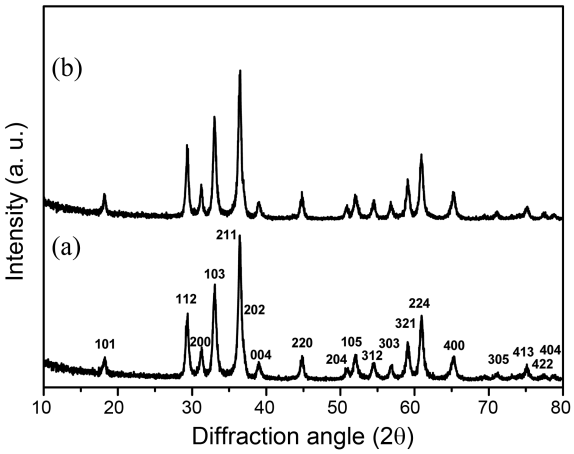

Figure 2. XRD patterns of the equimolar ZnO and Mn_2O_3 powder mixture milled for (a) 30 min and (b) 40 min, followed by annealing at 600 °C for 2 h in air.

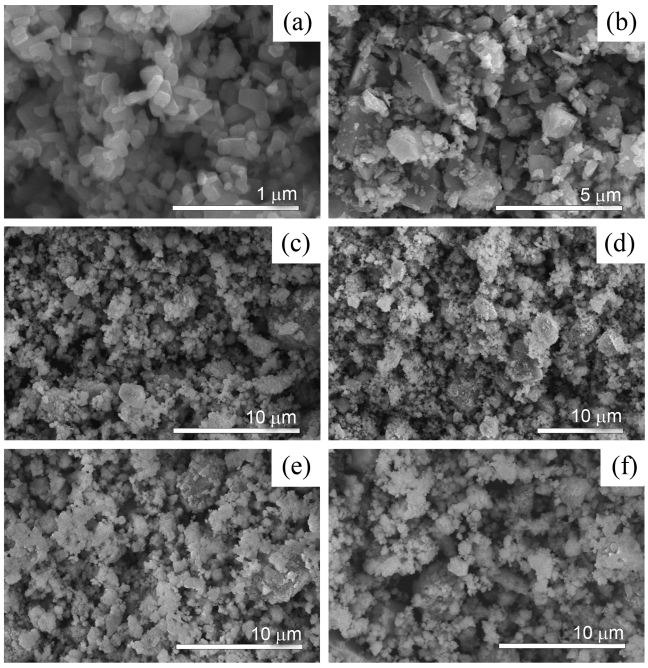

Figure 3. SEM micrographs of (a) ZnO; (b) Mn_2O_3; ball-milled samples after (c) 30 min and (d) 40 min; annealed samples after (e) 30 min and (f) 40 min ball-milling.

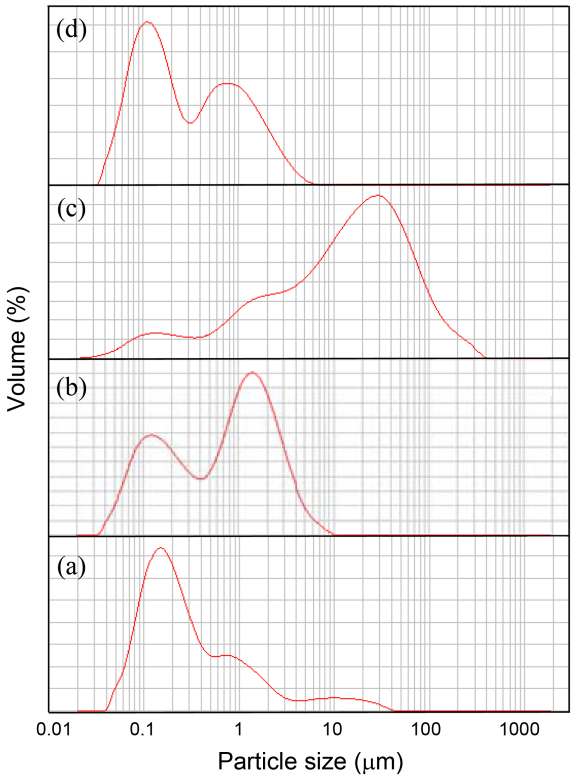

Figure 4. Particle size distribution of (a) ZnO; (b) Mn_2O_3 and 40 min ball-milled sample (c) before and (d) after 1 h of ultrasonication.

sample and annealed sample are given in Figure 3. The microstructure of the ball-milled powder shows the agglomerate structure of primary particles with submicron size. The annealed sample has a morphology similar to ball-milled powder. The size distribution of the starting materials and the ball-milled samples are presented in Figure 4, along with the size distribution of powders dispersed by an ultrasonic treatment for 2 h in ethanol, given as a comparison. The agglomeration of the ball-milled sample shows a spread distribution with a mean size of around 13 μm, while the ultrasonic treatment leads to a distribution consisting of peaks at 0.2 μm and 2 μm with a mean size of around 0.5 μm. Interestingly, it appears that the size distribution of the latter case (Fig. 4(d)) is similar to that of the starting material, Mn_2O_3 (Fig. 4(b)).

Electrochemical tests were performed using the mechanochemically synthesized $ZnMn_2O_4$ powders and the well-crystallized sample. Figure 5 shows the galvanostatic discharge-charge curves for the first two cycles of the ball-milled samples. The charge (lithiation)-discharge (delithiation) profiles are very similar to those of the nanocrystalline $ZnMn_2O_4$ electrode prepared by the polymer-pyrolysis method[9] and the flower-like $ZnMn_2O_4$ sample synthesized by the solvothermal process.[10] This infers that the $ZnMn_2O_4$ phase was successfully synthesized by the mechanochemical process. The first charge/discharge capacities and the initial coulombic efficiency for the 30 and 40 min ball-milled samples are 1202/773 mAh g^{-1}, 64.3% and 1271/810 mAh g^{-1}, 63.7%, respectively. The initial coulombic efficiencies are higher than those previously reported, cf. 58.8%[9] and 56.5%.[10] The high coulombic efficiency is attributed to the low specific surface area of the ball-milled sample compared with those of the nanocrystalline[9] and flower-like superstructures[10] as deduced from the particle size and morphology. The initial capacity loss of the $ZnMn_2O_4$ electrode during the first cycle is mainly due to the formation of the solid-electrolyte interphase layers at the $ZnMn_2O_4$/ electrolyte interface.[9,10] It is notable that the initial discharge capacity of the 40-min ball-milled sample is high compared with those of the 30-min ball-milled sample, and the nanocrystalline[9] and flower-like superstructures.[10] The reaction mechanism between Li and $ZnMn_2O_4$ during charge-discharge was proposed by Xiao *et al.*[10] as follows.

$$ZnMn_2O_4 + 8Li^+ + 8e^- \rightarrow Zn + 2Mn + 4Li_2O \quad (1)$$

$$Zn + Li^+ + e^- \leftrightarrow LiZn \quad (2)$$

$$2Mn + 2Li_2O \leftrightarrow 2MnO + 4Li^+ + 4e^- \quad (3)$$

$$Zn + Li_2O \leftrightarrow ZnO + 2Li^+ + 2e^- \quad (4)$$

$ZnMn_2O_4$ is reduced during the first discharge to form a

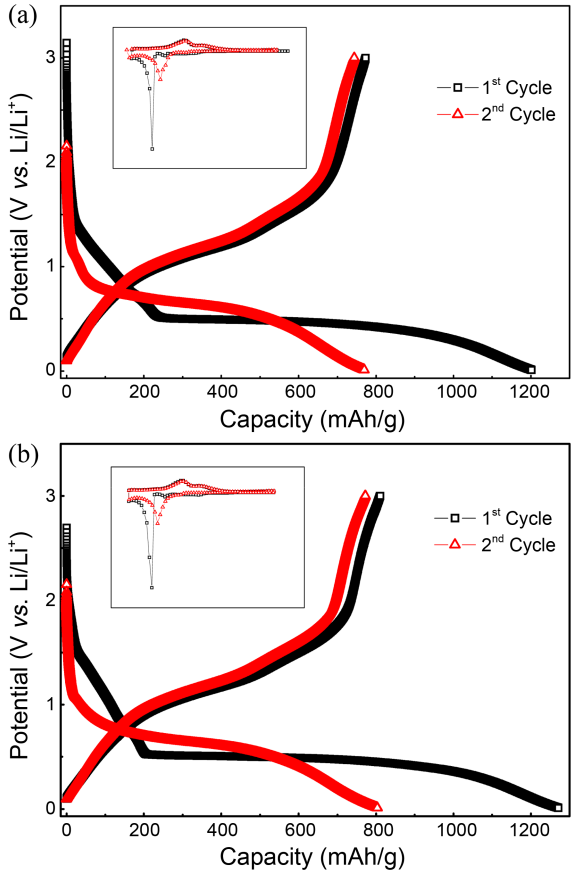

Figure 5. Discharge-charge profiles for the first two cycles of $ZnMn_2O_4$ prepared by (a) 30 min and (b) 40 min milling. The insets show the differential capacity (dQ/dV) *vs.* voltage curves for the first two cycles of each electrode.

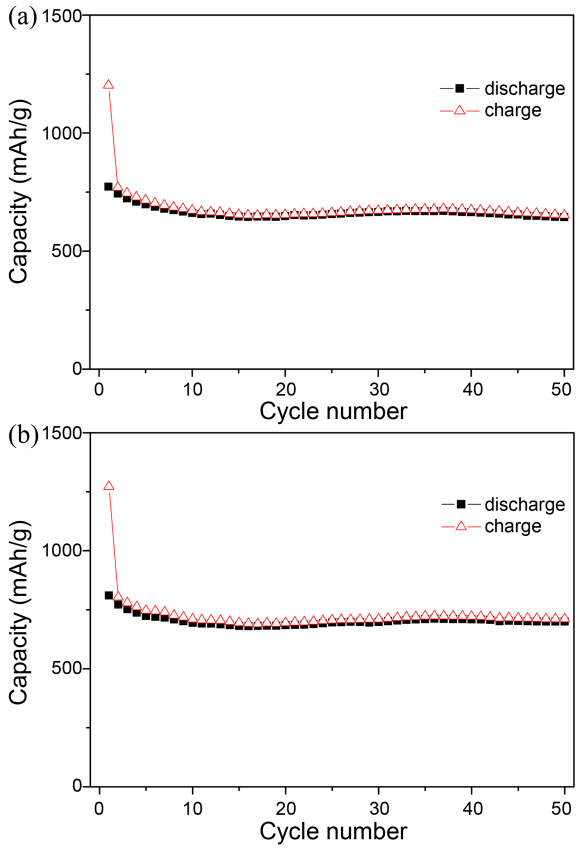

Figure 6. Cycle performance of $ZnMn_2O_4$ prepared by (a) 30 min and (b) 40 min milling.

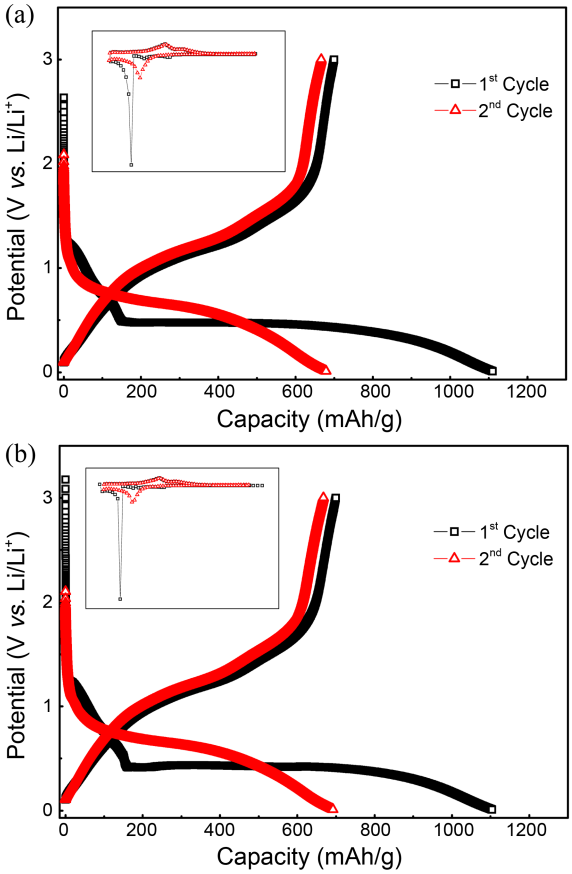

Figure 7. Discharge-charge profiles for the first two cycles of $ZnMn_2O_4$ prepared by (a) 30 min and (b) 40 min milling, followed by annealing at 600 °C for 2 h in air. The insets show the differential capacity (dQ/dV) *vs.* voltage curves for the first two cycles of each electrode.

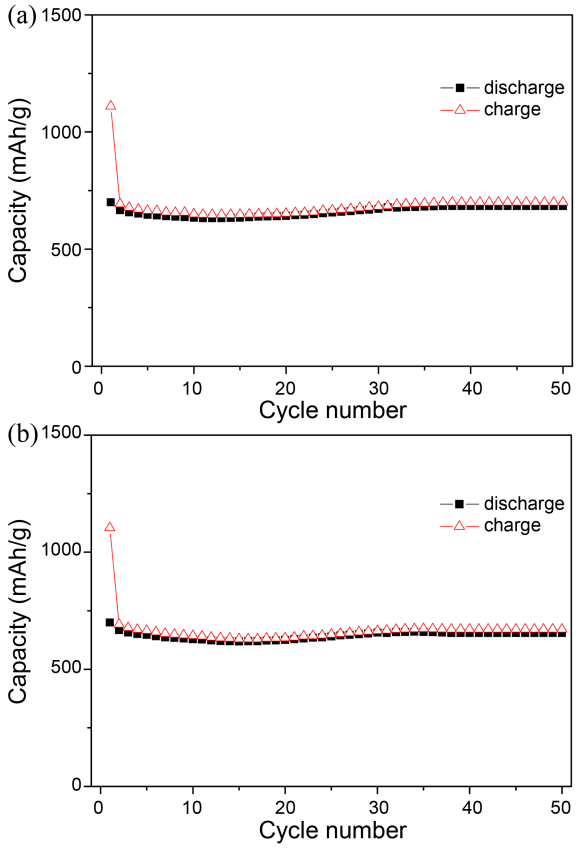

Figure 8. Cycle performance of $ZnMn_2O_4$ prepared by (a) 30 min and (b) 40 min milling, followed by annealing at 600 °C for 2 h in air.

nanocomposite of Zn, Mn and Li_2O according to Eq. (1). After the first cycle, reversible electrode reactions take place according to Eqs. (2)-(4), which leads to a theoretical capacity of 784 mAh g^{-1}. The initial discharge capacity of ball-milled samples appears to be similar to the theoretical capacity. Nevertheless, the high storage capacity of the ball-milled samples may seem to be attributed to the Fe contamination by the steel container and balls during ball milling, although a detailed study is needed to confirm the exact mechanism.

In the case of Fe and Fe_2O_3, the following reversible reaction is proposed.[12,13]

$$2Fe + 3Li_2O \leftrightarrow Fe_2O_3 + 6Li^+ + 6e^- \quad (5)$$

The charge-discharge capacities of the ball-milled sample electrodes as a function of cycle number are presented in Figure 6. Similar to those in previous studies,[9,10] the capacities gradually decrease up to around 10 cycles, after which the capacity retention is stabilized. After 50 cycles, the reversible capacity is as high as 645 and 700 mAh g^{-1}, for the 30-min and 40-min ball-milled samples, respectively, and the latter is much higher than 569 mAh g^{-1} of nanocrystalline[9] and 626 mAh g^{-1} of flower-like superstructures.[10]

Figure 7 shows the charge-discharge curves for the first two cycles of the well-crystallized $ZnMn_2O_4$ electrode. The charge-discharge profiles are very similar to those of the ball-milled powder electrode. The similarities between the electrodes are apparent in the differential capacity plots, as shown in the insets of Figure 5 and 7. In the annealed samples the cycling performance is excellent as shown in Figure 8, and its initial discharge capacity is a little bit lower than that of the ball-milled electrodes.

Conclusions

The mechanochemical process was applied for preparing $ZnMn_2O_4$ by direct reaction of the constituent oxides at room temperature. High-energy ball milling leads to a solid-state reaction for the formation of $ZnMn_2O_4$, which is achieved in a short time (30 min). The discharge-charge profiles of the ball-milled samples are very similar to those of the nanocrystalline $ZnMn_2O_4$ electrodes prepared using the polymer-pyrolysis method and the flower-like $ZnMn_2O_4$ synthesized by the solvothermal process. The ball-milled samples show an enhanced initial coulombic efficiency, high reversible capacity, and stable capacity retention with cycling. These results demonstrate that mechanochemically synthesized $ZnMn_2O_4$ is very promising as a high-capacity anode material for lithium-ion batteries.

Acknowledgments. This study was supported by the National Research Foundation of Korea Grant funded by the Korean Government (MEST) (NRF-2009-C1AAA001-0093307).

References

1. Poizot, P.; Laruelle, S.; Grugeon, S.; Dupont, L.; Tarascon, J. M. *Nature* **2000**, *407*, 496.
2. Lou, X. W.; Deng, D.; Lee, J. Y.; Feng, J.; Archer, L. A. *Adv. Mater.* **2008**, *20*, 258.
3. Bruce, P. G.; Scrosati, B.; Tarascon, J. M. *Angew. Chem. Int. Ed*. **2008**, *47*, 2.
4. Sharma, Y.; Sharma, N.; Rao, G. V. S.; Chowdari, B. V. R. *Adv. Funct. Mater.* **2007**, *17*, 2855.
5. Pasero, D.; Reeves, N.; West, A. R. *J. Power Sources* **2005**, *141*, 156.
6. Reddy, B. M. V.; Yu, T.; Sow, C. H.; Shen, Z. X.; Lim, C. T.; Subba Rao, G. V.; Chowdari, B. V. R. *Adv. Funct. Mater.* **2007**, *17*, 272.
7. Fan, Q.; Whittingham, M. S. *Electrochem. Solid-State Lett*. **2007**, *10*, A48.
8. Nam, K. T.; Kim, D. W.; Yoo, P. J.; Chiang, C. Y.; Meethong, N.; Hammon, P. T.; Chiang, Y. M.; Belcher, A. M. *Science* **2006**, *312*, 885.
9. Yang, Y.; Zhao, Y.; Xiao, L.; Zhang, L. *Electrochem. Commun.* **2008**, *10*, 1117.
10. Xiao, L.; Yang, Y.; Yin, J.; Li, Q.; Zhang, L. *J. Power Sources* **2009**, *194*, 1089.
11. Suryanarayana, C. *Prog. Mater. Sci.* **2001**, *46*, 1, and references therein.
12. Sharma, V Y.; Sharma, N.; Subba Rao, G. V.; Chowdari, B. V. R. *Electrochim. Acta* **2008**, *53*, 2380.
13. Guo, X.; Lu, X.; Fang, X.; Mao, Y.; Wang, Z.; Chen, L.; Xu, X.; Yang, H.; Liu, Y. *Electrochem. Commun.* **2010**, *12*, 847.